Scientific Research Publishing

International Journal of Astronomy and Astrophysics, 2023, 13, 298-310
https://www.scirp.org/journal/ijaa
ISSN Online: 2161-4725
ISSN Print: 2161-4717

Transport in Astrophysics: V. On the Red Sun at Horizon

Lorenzo Zaninetti

Physics Department, University of Turin, Turin, Italy
Email: l.zaninetti@alice.it

How to cite this paper: Zaninetti, L. (2023) Transport in Astrophysics: V. On the Red Sun at Horizon. *International Journal of Astronomy and Astrophysics*, **13**, 298-310.
https://doi.org/10.4236/ijaa.2023.134017

Received: November 21, 2023
Accepted: December 22, 2023
Published: December 25, 2023

Abstract

In order to simulate the red sun at the horizon we need to evaluate the average density of matter along a line of sight characterized by a given elevation angle. The decrease in frequency or the increase in wavelength of the light is modeled by the Bouguer-Beer-Lambert law and as a consequence, all the Planck spectrum is shifted toward lower frequencies or longer wavelengths.

Keywords

Solar System, General, Earth

1. Introduction

The red color of the sun at the horizon raises some astrophysical questions that should be solved:

1) What is the mechanism that changes the color of the sun from yellow to red?

2) What is the role of the declination angle in this change of color?

The solar spectrum at the top of the atmosphere is here assumed to be modeled by the Planck distribution which dates back to 1901 [1]. The Planck distribution is an active field of research and we select some topics under discussion: A careful examination of the maximum in emissivity in the following domains: frequencies, wavelength and wave number [2]; a parametrization of the peaks in emissivity with the Lambert function [3]; a parametrization of the fraction of the total power emitted by a blackbody in a given spectral band with the polylogarithm function [4]; a semi-analytical method to calculate the total radiance received from a black body between two frequencies [5]; a careful analysis of the Planck distribution in order to explain three features of the Solar photons: refrangibility, heat effect and chemical effect [6]. In order to answer the posed questions, we review in Section 2 the existing data on the density of the atmos-

phere and we analyze in Section 3 the behavior of the density of matter along three lines of sight: horizon, zenith and variable declination angle. The losses in energy along the line of sight are evaluated in the framework of a blackbody distribution for frequencies, see Section 4, and a blackbody distribution for wavelengths, see Section 5. Section 6 derives the temperature of the sun's spectrum for the air mass zero (AM0).

2. The Density Profile of the Atmosphere

We assume that the atmosphere has a density of the type

$$\rho(r) = C_{atm} * \exp\left(-\frac{r}{s}\right), \tag{1}$$

where r is the altitude above the sea level, C_{atm} and s are two numerical parameters to be found from the available data. In order to find the above parameters we processed the data of the U.S. standard atmosphere as reported in https://www.engineeringtoolbox.com/. Conversely a ray of the sun in the travel from the top of the atmosphere interacts with a growing density of air

$$\rho(r) = C_{out} * \exp\left(\frac{r}{s}\right), \tag{2}$$

where C_{out} is a constant and r varies between 0 at the top of the atmosphere and t, the thickness of the atmosphere. In both cases r is evaluated along a line which crosses the center of Earth and Table 1 reports the numerical values for the atmosphere here adopted. A first application is the average density of the atmosphere evaluated along the two directions of a radial line which crosses the center of Earth

$$\overline{\rho_{zenith}} = \frac{\int_0^t C_{atm} * \exp\left(-\frac{r}{s}\right) dr}{t} = \frac{\int_0^t C_{out} * \exp\left(\frac{r}{s}\right) dr}{t} = 0.127892 \frac{\text{kg}}{\text{m}^3}. \tag{3}$$

The above result means that the average density at zenith is equal in both directions.

Table 1. Numerical values for the parameters in SI.

symbol	meaning	numerical value
C_{atm}	constant from inside	1.44766271 kg/m^3
C_{out}	constant from outside	$1.75711175 \times 10^{-5}$ kg/m^3
s	atmospheric scale	7067.63477 m
t	thickness atmosphere	8×10^4 m
a	radius Earth	6.3781×10^6 m
l_{zenith}	line of sight for zenith	8×10^4 m
$l_{horizon}$	line of sight for horizon	1.0133×10^6 m
$\overline{\rho_{zenith}}$	averaged density along zenith	0.127892 kg/m^3
$\overline{\rho_{horizon}}$	averaged density along horizon	0.380299 kg/m^3

3. The Involved Geometry

We start with the observer situated on the Earth's surface at the center of an X-Y frame with coordinates (0, 0). A first line represents the line of sight of the sun

$$y = \tan(\theta)x, \tag{4}$$

where the angle θ in rad grows in the counterclockwise direction. The sun at the horizon has an angle $\theta = 0$ and sun at the zenith has an angle $\theta = \frac{\pi}{2}$; in astronomy θ is named elevation angle.

A second line

$$y = \tan(\phi)x - a, \tag{5}$$

crosses the center of the Earth $(0, -a)$ with a representing the Earth's radius, see the numerical value in Table 1, and ϕ a counter-clockwise angle in rad. The two lines are reported in Figure 1. A first circle represents the Earth's surface

$$(y+a)^2 + x^2 = a^2, \tag{6}$$

and a second circle represents the end of the atmosphere

$$(y+a)^2 + x^2 = (a+t)^2. \tag{7}$$

We now analyze two directions of sight, zenith and horizon, and then the line of sight as function of the angle of sight θ.

3.1. Two Directions

We limit ourselves to the zenith, $\theta = \frac{\pi}{2}$, and to the horizon, $\theta = 0$, in order to

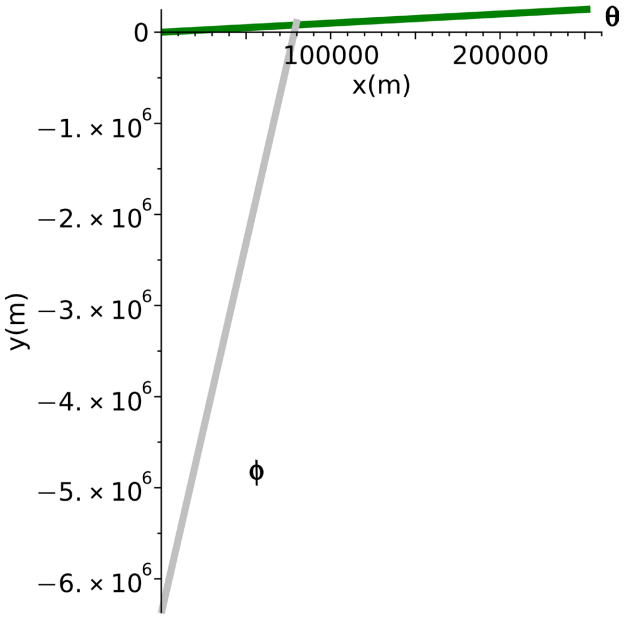

Figure 1. The first green line of sight with gradient equal to $\tan(\theta)$ and the second gray line which connects the center of Earth to the atmosphere, gradient equal to $\tan(\phi)$.

obtain first results in a simple way. The intersection of the line $y=0$ with the second circle (7), $x_{\max}$ is at

$$x_{\max}=\sqrt{2at+t^2}, \tag{8}$$

which means that at the horizon the line of sight is ≈12.6 bigger in respect to the zenith. A way to parameterize the second line, see Equation (5), which crosses the center of the Earth is

$$y=\frac{a\left(x-x_h\right)}{x_h}, \tag{9}$$

where x_h is the intercept with the line $y=0$ which varies between 0 and $x_{\max}$, see Equation (8). The distance as going from outside to inside in the atmosphere along the above line to the line $y=0$ is function of x_h

$$\Delta r=t-\sqrt{\left(x_h-\frac{x_h a}{\sqrt{a^2+x_h^2}}\right)^2+\frac{a^2\left(-\sqrt{a^2+x_h^2}+a\right)^2}{a^2+x_h^2}}. \tag{10}$$

When $x_h=x_{\max}$ we have $\Delta r=0$ and when $x_h=0$ we have $\Delta r=t$; **Figure 2** reports an example of evaluation of Δr.

A second application is the average density of the atmosphere evaluated along the line of sight for the horizon which is

$$\overline{\rho_{horizon}}=\frac{1}{\sqrt{2at+t^2}}\int_0^{\sqrt{2at+t^2}} C_{out}\,\mathrm{e}^{\frac{t-\sqrt{\left(x-\frac{xa}{\sqrt{a^2+x^2}}\right)^2+\frac{a^2\left(-\sqrt{a^2+x^2}+a\right)^2}{a^2+x^2}}}{s}}=0.380299\,\frac{\mathrm{kg}}{\mathrm{m}^3}. \tag{11}$$

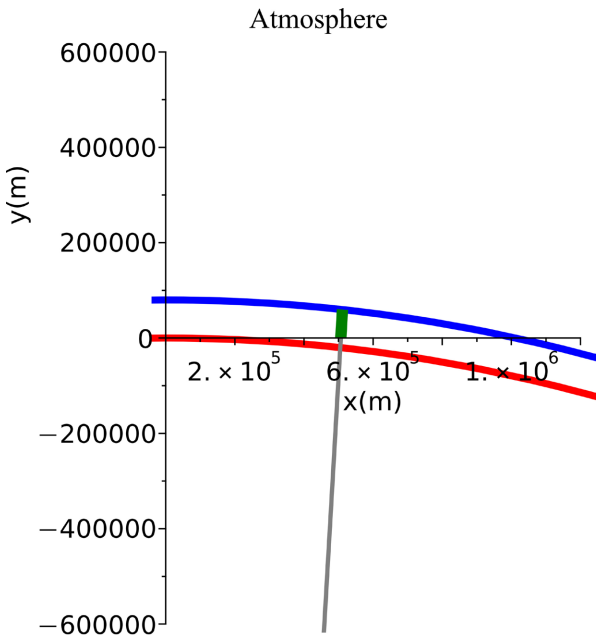

Figure 2. First circle in red, second circle in blue, line which connect the center of Earth to $y=0$ in gray and thick line which represents the distance on which to evaluate the density in green.

The above numerical result allows to say that the average density along the line of sight for the horizon is ≈2.97 time bigger than that along the line of sight of the zenith. The line of sight along the zenith direction is $l_{zenith} = t$ and along the horizon direction is $l_{horizon} = x_{\max}$.

3.2. Variable Angle of Sight

The angle θ characterizes the line of sight, see Equation (4), and the intersection of the above line with the second circle, see Equation (7), ($x_{s,2}$, $y_{s,2}$), is at

$$x_{s,2} = \left(\sqrt{\left(\sin^2(\theta)a^2 + 2at + t^2\right)\sec^2(\theta)}\cos(\theta) - \sin(\theta)a\right)\cos(\theta) \tag{12}$$

$$y_{s,2} = \sqrt{\sin^2(\theta)a^2 + 2at + t^2}\sin(\theta) - \sin^2(\theta)a. \tag{13}$$

The second line which crosses the center of the Earth, see Equation (5), has a minimum angle ϕ

$$\phi_{\min} = \arctan\left(\frac{\sqrt{\sin^2(\theta)a^2 + 2at + t^2}\tan(\theta) + a\cos(\theta)}{-\sin(\theta)a + \sqrt{\sin^2(\theta)a^2 + 2at + t^2}}\right), \tag{14}$$

which means that the range of ϕ is $\left[\phi_{\min}, \frac{\pi}{2}\right]$ and **Figure 3** reports the value of $\phi_{\min}$ as function of the angle θ in degree.

The intersection, ($x_{s,e}$, $y_{s,e}$), between the line which represents the line of sight, see Equation (4), and that one which represents the radial direction in respect to the center of Earth, see Equation (5), is at

$$x_{s,e} = -\frac{a}{\tan(\theta) - \tan(\phi)} \tag{15}$$

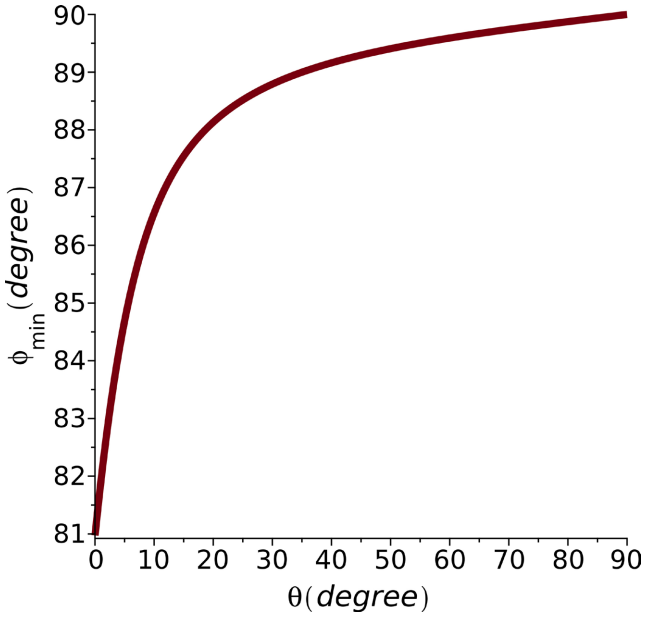

Figure 3. The value of $\phi_{\min}$ as function of the angle θ in degree, parameters as in **Table 1**.

$$y_{s,e} = -\frac{\tan(\theta)a}{\tan(\theta)-\tan(\phi)}. \tag{16}$$

The intersection, ($x_{e,c}$, $y_{e,c}$), between the line which represents the radial direction in respect to the center of Earth, see Equation (5), and the second circle, see Equation (7), is at

$$x_{e,c} = \frac{\sqrt{\left(2at+t^2\right)\sec^2(\phi)+\tan^2(\phi)a^2+a^2}}{\tan^2(\phi)+1} \tag{17}$$

$$y_{e,c} = \frac{\tan(\phi)\sqrt{\left(2at+t^2\right)\sec^2(\phi)+\tan^2(\phi)a^2+a^2}}{\tan^2(\phi)+1} - a. \tag{18}$$

As a consequence of the above intersection the distance Δr as evaluated on line crossing the Earth from outside the atmosphere to the intersection of the two lines is

$$\Delta r = \sqrt{\frac{\left(\tan^2(\phi)a-\tan(\phi)A+A\tan(\theta)+a\right)^2}{\left(\tan^2(\phi)+1\right)\left(\tan(\phi)-\tan(\theta)\right)^2}}, \tag{19}$$

where

$$A = \sqrt{(a+t)^2\sec^2(\phi)}. \tag{20}$$

We are now ready to evaluate the average density of the atmosphere along the line of sight θ which is defined as

$$\overline{\rho(\theta)} = \frac{\int_{\phi_{\min}}^{\frac{\pi}{2}} C_{out} \mathrm{e}^{\frac{\sqrt{\left(\left(-\tan(\phi)+\tan(\theta)\right)\sqrt{(a+t)^2\sec^2(\phi)}+\left(\tan^2(\phi)+1\right)a\right)^2}}{\left(\tan^2(\phi)+1\right)\left(\tan(\phi)-\tan(\theta)\right)^2}}}{s} \mathrm{d}\phi}{\frac{\pi}{2}-\phi_{\min}}, \tag{21}$$

whith $\phi_{\min}$ as given by Equation (14). The above integral does not have an analytical solution and therefore we introduce the following fit for the numerical integration

$$\overline{\rho(\theta)} \approx 0.131733 + 0.244471\mathrm{e}^{-0.37047\theta(\text{degree})}, \tag{22}$$

see Figure 4. The percentage error of the fit, δ , is $\delta = 1.07\%$ at $\theta = 0$ degree and $\delta = 3\%$ at $\theta = 90$ degree.

4. The Planck Distribution in Frequencies

The Planck distribution for the spectral radiance [1] [7], B_ν , is

$$B_\nu = \frac{2h\nu^3}{c^2\left(\mathrm{e}^{\frac{h\nu}{kT}}-1\right)}\frac{\mathrm{J}}{\mathrm{s}\cdot\mathrm{m}^2\cdot\mathrm{sr}\cdot\mathrm{Hz}}, \tag{23}$$

where ν is the frequency, c the light velocity, h the Planck constant, T the temperature and k the Boltzmann constant. The numerical values of the above physical constants are reported in Table 2 in SI units [8].

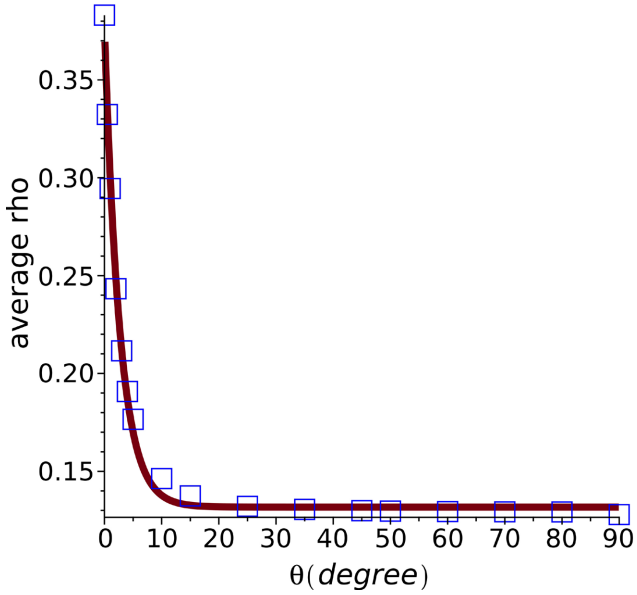

Figure 4. The value of the average density of the atmosphere as function of the angle θ in degree, parameters as in **Table 1**. The red full line represents the fit as given by Equation (22) and the blue square the numerical integration.

Table 2. Numerical values for the parameters connected with the Planck distribution in SI.

symbol	meaning	numerical value
c	light velocity	299,792,458 m/s
h	Planck constant	$6.62607015 \times 10^{-34}$ J/Hz
k	Boltzman constant	1.380649×10^{-23} J/K
T	Temperature of the sun	5772 K
ν_{yellow}	frequency of the color yellow	520×10^{12} Hz
ν_{red}	frequency of the color red	440×10^{12} Hz
μ	coefficient of attenuation for frequencies	4.4×10^{-7} m^2/kg

The spectral radiance has a maximum, $\nu_{\max}$, at

$$\nu_{\max} = \frac{kT\left(W\left(-3e^{-3}\right)+3\right)}{h} \tag{24}$$

where W is the Lambert W function, after [9]; with the data of **Table 2**. $\nu_{\max} = 3.3933 \mp 10^{14}$ Hz which is in the near infrared region. We now analyze how is possible to decrease the frequency of the sun at zenith characterized by the yellow color with frequency ν_{yellow} to the red frequency, ν_{red}, at horizon, see **Table 2** for the numerical values. The ratio $\frac{\nu_{red}}{\nu_{yellow}} = 0.8461$, see parameters in **Table 2**, is the target of the following simulation. The Bouguer-Beer-Lambert law [10] [11] [12] is very useful in spectrophotometry

$$I(d) = I_0 \exp -\alpha d, \tag{25}$$

where I_0 is the initial intensity of the light, I is the intensity of the light after traveling the distance d and α is a coefficient of absorption expressed in unit neper, see formula (1) in [13]. The parameter α can be expressed as

$$\alpha = c_a c_b, \tag{26}$$

where c_b is a coefficient of attenuation and c_a the concentration. Here we assume that the energy E of a photon which travels the atmosphere decreases according to the following ODE

$$\frac{\mathrm{d}}{\mathrm{d}x} E(x) = -\mu \rho_{ave} E(x), \tag{27}$$

where ρ_{ave} is the averaged density of matter in kg/m^3 and μ the attenuation coefficient for energy in m^2/kg. A usual assumption is $E = h\nu$ which produces the following ODE in frequency

$$\frac{\mathrm{d}}{\mathrm{d}x} \nu(x) = -\mu \rho_{ave} \nu(x), \tag{28}$$

see formula (5) in [14]. The above ODE is solved assuming the initial condition $\nu(0) = \nu_0$

$$\nu(x) = \nu_0 \mathrm{e}^{-\mu \rho_{ave} x}. \tag{29}$$

Figure 5 reports the decrease in frequency at the zenith which is minimum and Figure 6 reports the decrease in frequency at the zenith which covers the yellow-red transition.

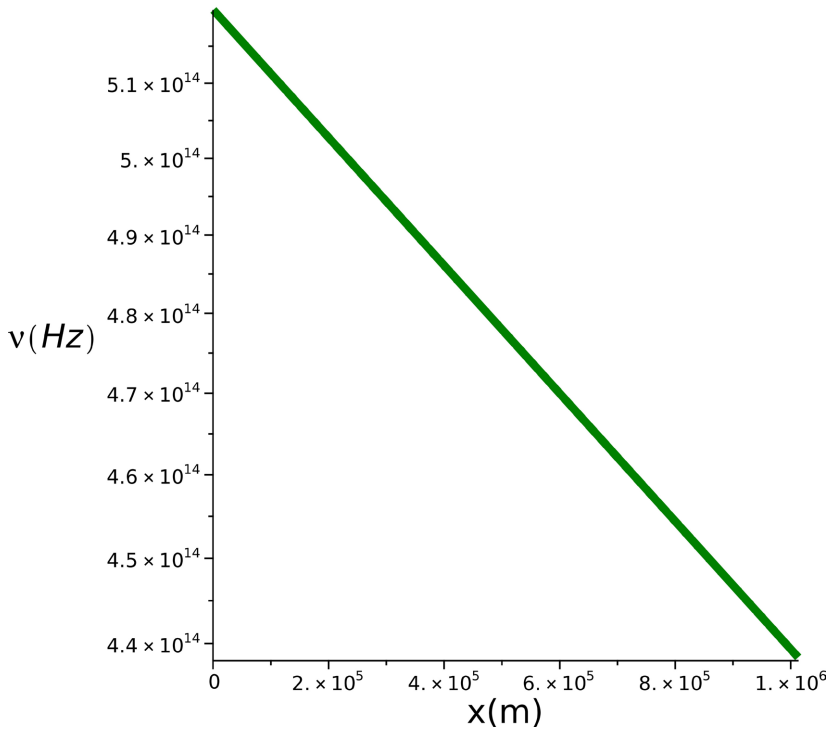

Figure 5. The decrease in frequency as function of the distance at the zenith, ($\theta = \frac{\pi}{2}$), parameters as in Table 1.

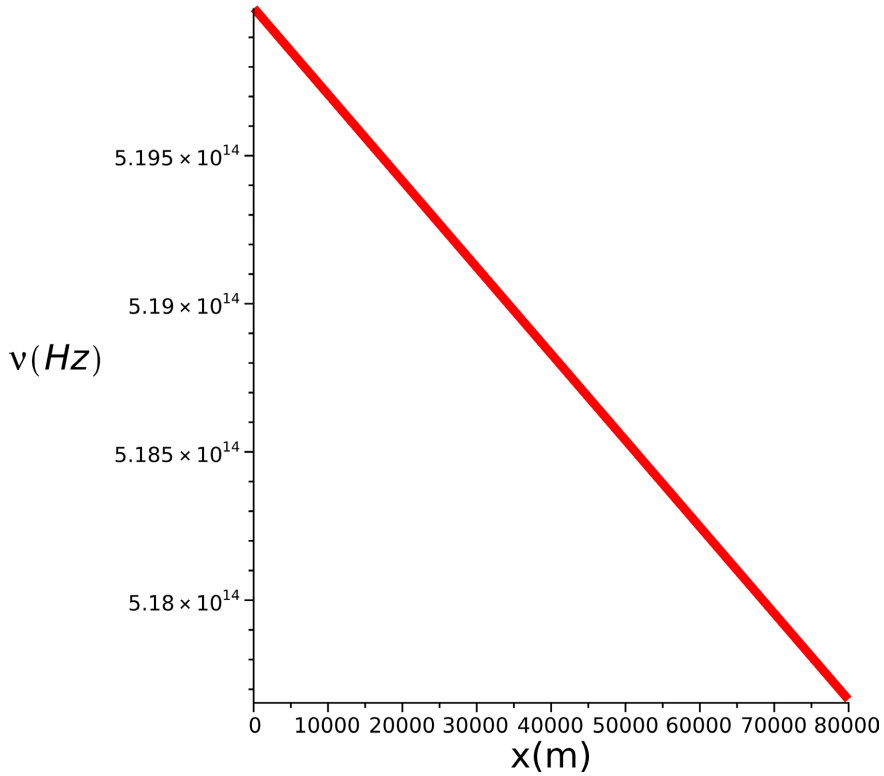

Figure 6. The decrease in frequency as function of the distance at horizon, ($\theta = 0$), parameters as in **Table 1**.

We are now ready to display the evolution of the spectral radiance adopting the following rules:

1) We select an initial frequency at the top of the atmosphere.

2) We evaluate the spectral radiance for the initial frequency.

3) We evaluate the final frequency in a given direction with formula (29) adopting the appropriate density and line of sight which are functions of the angle θ.

4) The spectral radiance of the final frequency is that of the initial frequency evaluated at point [2].

As an example, **Figure 7** reports the overall spectral radiance in three directions of sight.

5. The Planck Distribution in Wavelengths

The Planck distribution in wavelengths is

$$B_\lambda = \frac{2hc^2}{\lambda^5\left(e^{\frac{hc}{\lambda kT}} - 1\right)}, \tag{30}$$

and the maximum, λ_{max}, is at

$$\lambda_{max} = \frac{hc}{Tk\left(W\left(-5e^{-5}\right) + 5\right)}. \tag{31}$$

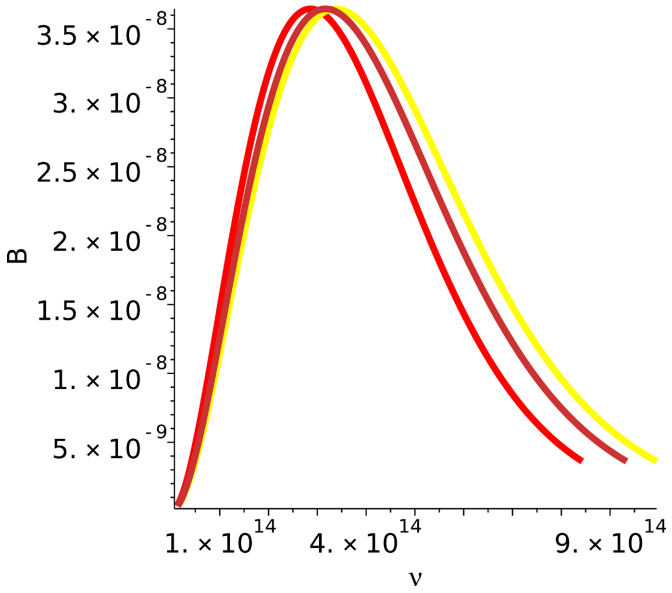

Figure 7. The modified spectral radiance at the horizon ($\theta = 0$ degree), red line, at $\theta = 3$ degree, orange line and at the zenith ($\theta = 0$ degree), yellow line.

As a practical application at the temperature here adopted of 5772 K the maximum of the radiance is at 502.039×10^{-9} m or 502.039 nm. We start from Equation (28) in order to obtain the ODE for the increase in wavelength

$$\frac{\mathrm{d}}{\mathrm{d}x}\lambda(x) = \lambda(x)\mu\rho_{ave}. \tag{32}$$

The above ODE is solved assuming the initial condition $\lambda(0) = \lambda_0$

$$\lambda(x) = \lambda_0 \mathrm{e}^{\mu\rho_{ave}x}. \tag{33}$$

We are now ready to display the evolution of the spectrum adopting the following rules:

1) We select an initial wavelength at the top of the atmosphere.

2) We evaluate the spectral radiance for the initial wavelength.

3) We evaluate the final wavelength in a given direction with formula (33) adopting the appropriate density and line of sight which are functions of the angle θ.

4) The spectral radiance of the final wavelength is that of the initial wavelength evaluated at point [2].

As an example **Figure 8** reports the overall spectrum on three directions of sight.

6. Temperature Determination

The solar cell measurements require an accurate knowledge of the solar spectrum at the top of the atmosphere, as an example at 35 km, which is called air mass zero (AM0) [15]. The data of AMO can be found, as an example, digitizing ASTM E-490 on a search engine, and are displayed as a green point in **Figure 9**. We fit the AM0 data with the following function

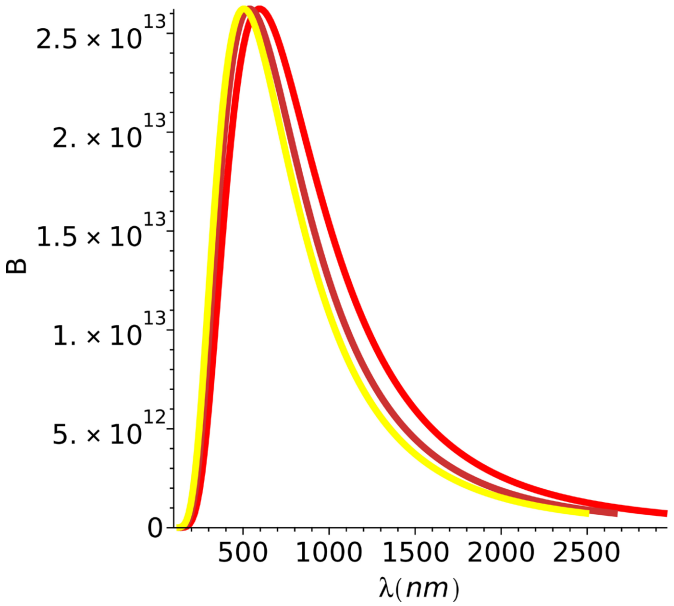

Figure 8. The theoretical spectrum at the horizon ($\theta = 0$ degree), red line, at $\theta = 3$ degree, orange line and at the zenith ($\theta = 0$ degree), yellow line, the wavelengths are expressed in nm.

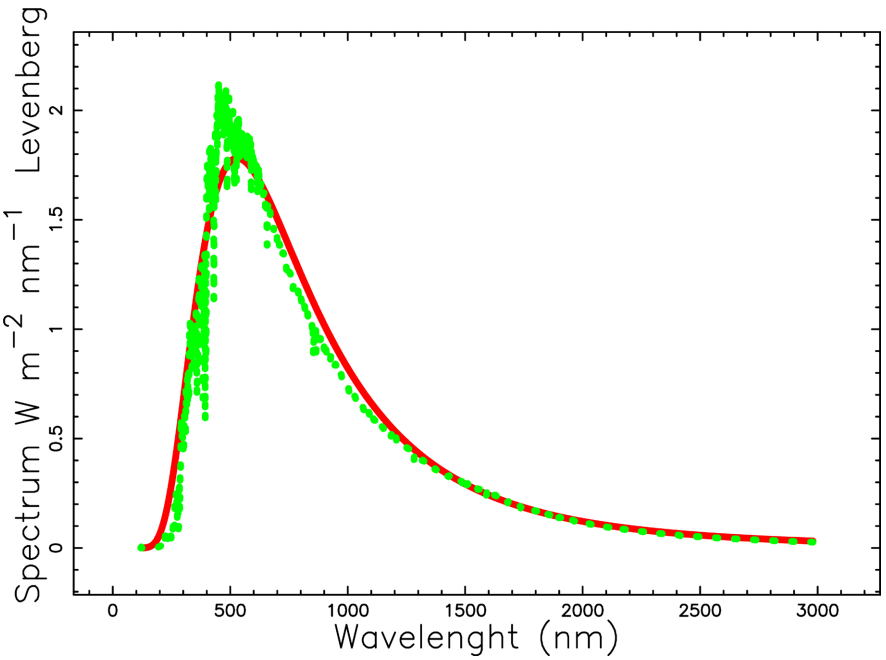

Figure 9. Spectral radiance versus wavelength in nm for AM0, green points, and theoretical fit, red line.

$$f(\lambda,T) = B \times \frac{2hc^2}{\lambda^5\left(e^{\frac{hc}{\lambda kT}} - 1\right)}, \tag{34}$$

where B is a constant which allows to match the data. The temperature and the constant can be found through the Levenberg-Marquardt method (subroutine

MRQMIN in [16]) and turn out to be $T = 5467.49\,\mathrm{K}$ and $A = 8.9033 \times 10^{-14}$. The above value of temperature has a percent error of 5.27% on the value here adopted of 5772 K.

7. Conclusions

The average density of the atmosphere

The evaluation of the average density of the atmosphere is simple along a radial direction which crosses the center of Earth but complicated along a given elevation angle, see Equation (22) for a numerical approximation.

The decrease in frequencies

The ODE for the decrease in frequency due to the Bouguer-Beer-Lambert law, see Equation (28), allows the yellow-red transition for the sun at the horizon. Due to the fact that the initial value of the spectral radiance is maintained, all the spectrum is shifted toward lower frequencies, see as an example **Figure 7**.

The increase in wavelengths

The ODE for the increase in wavelengths, see Equation (33), explains the yellow-red transition. Also here the initial value of the spectral radiance is maintained and as a consequence all the spectrum is shifted toward bigger wavelengths, see as an example **Figure 8**.

Conflicts of Interest

The author declares no conflicts of interest regarding the publication of this paper.

References

[1] Planck, M. (1901) Ueber das Gesetz der Energieverteilung im Normalspectrum. *Annalen der Physik*, **309**, 553-563. https://doi.org/10.1002/andp.19013090310

[2] Kramm, G. and Mölders, N. (2009) Planck's Blackbody Radiation Law: Presentation in Different Domains and Determination of the Related Dimensional Constants. https://arxiv.org/vc/arxiv/papers/0901/0901.1863v1.pdf

[3] Stewart, S.M. (2011) Wien Peaks and the Lambert W Function. *Revista Brasileira de Ensino de Fsica*, **33**, 6 p. https://doi.org/10.1590/S1806-11172011000300008

[4] Stewart, S.M. (2012) Spectral Peaks and Wien's Displacement Law. *Journal of Thermophysics and Heat Transfer,* **26**, 689. https://doi.org/10.2514/1.T3789

[5] Calcaneo-Roldan, C., Salcido, O. and Santana, D. (2017) A Semi-Analytical Approach to Black Body Radiation. *European Journal of Physics*, **38**, 055807. https://doi.org/10.1088/1361-6404/aa7d1d

[6] Stávek, J. (2023) What Is Hidden in the Planck Distribution Function and the Wien's Peaks? I. Three Features of the Solar Photons. *European Journal of Applied Physics*, **5**, 1. https://doi.org/10.24018/ejphysics.2023.5.2.240

[7] Planck, M. (1959) The Theory of Heat Radiation. Dover Publications, New York.

[8] Mohr, P.J., Newell, D.B. and Taylor, B.N. (2016) CODATA Recommended Values of the Fundamental Physical Constants: 2014. *Reviews of Modern Physics*, **88**, 035009. https://doi.org/10.1103/RevModPhys.88.035009

[9] Lambert, J.H. (1758) Observations Variae in Mathesin Puram. *Acta Helvitica*,

Physico-Mathematico-Anatomico-Botanico-Medica, **3**, 128-168.

[10] Bouguer, P. (1729) Essai d'optique sur la gradation de la lumière. Claude Jombert, Paris.

[11] Lambert, J.H. (1760) Photometria sive de mensura et gradibus luminis, colorum et umbrae.

[12] Beer, A. (1852) Bestimmung der Absorption des rothen Lichts in farbigen Flüssigkeiten. *Annalen der Physik*, **162**, 78-88. https://doi.org/10.1002/andp.18521620505

[13] Mayerhöfer, T.G., Pahlow, S. and Popp, J. (2020) The Bouguer-Beer-Lambert Law: Shining Light on the Obscure *ChemPhysChem*, **21**, 2029-2046. https://doi.org/10.1002/cphc.202000464

[14] Kragh, H. (2017) Is the Universe Expanding? Fritz Zwicky and Early Tired-Light Hypotheses. *Journal of Astronomical History and Heritage*, **20**, 2-12. https://doi.org/10.3724/SP.J.1440-2807.2017.01.01

[15] Xu, G., Ke, Z., Zhuang, C., Li, Y., Cai, R., Yang, Y. and Du, X. (2023) Measurements and Analysis of Solar Spectrum in Near Space. *Energy Reports*, **9**, 1764-1173. https://doi.org/10.1016/j.egyr.2023.04.229

[16] Press, W.H., Teukolsky, S.A., Vetterling, W.T. and Flannery, B.P. (1992) Numerical Recipes in FORTRAN. The Art of Scientific Computing. Cambridge University Press, Cambridge, UK.